Cellulose
https://doi.org/10.1007/s10570-020-03223-5

ORIGINAL RESEARCH

High aspect ratio cellulose nanofibrils from macroalgae *Laminaria hyperborea* cellulose extract via a zero-waste low energy process

Amaka J. Onyianta · Dominic O'Rourke · Dongyang Sun · Carmen-Mihaela Popescu · Mark Dorris

Received: 14 January 2020 / Accepted: 8 May 2020

Abstract Homogeneous high aspect ratio cellulose nanofibrils (CNFs) were prepared from *Laminaria hyperborea* (LH) seaweed cellulose without any initial mechanical, biological or chemical pre-treatments. Fourier-transform infrared spectrophotometry revealed that LH cellulose was of the cellulose I_α allomorph, typical of algal cellulose. Compared with wood derived CNF, significant enhancements in crystallinity, viscoelastic properties, water retention values (WRV) and morphological characteristics were identified with a single pass at 1 wt. % cellulose content through a high-pressure homogeniser. Further mechanical fibrillation did not lead to appreciable improvements in material properties that would justify the added energy consumption, which at a single pass is at least a factor of 10 lower than with wood cellulose processing. Good quality CNFs with little compromise in material properties were also obtainable at 2–3 wt. % cellulose contents as identified from viscoelastic analysis, WRV and morphological analysis. LHCNFs also showed good thermal stability, which in summary presents a multifunctional high value cellulose nanomaterial that can find application in various fields.

A. J. Onyianta (✉) · D. O'Rourke · D. Sun · M. Dorris
Nanomaterial Unit, School of Engineering and Built Environment, Edinburgh Napier University, Edinburgh, UK
e-mail: a.onyianta@napier.ac.uk

D. O'Rourke
e-mail: d.orourke@napier.ac.uk

D. Sun
e-mail: d.sun@napier.ac.uk

M. Dorris
e-mail: m.dorris@napier.ac.uk

C.-M. Popescu
Petru Poni Institute of Macromolecular Chemistry of the Romanian Academy, Iasi, Romania
e-mail: mihapop@icmpp.ro

Published online: 13 July 2020

Graphic abstract

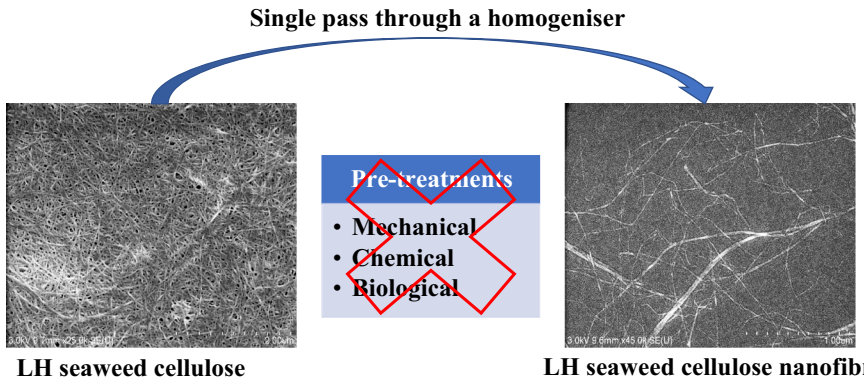

Keywords Cellulose nanofibrils (CNFs) · Algae cellulose · CNF viscoelastic properties · CNF morphological properties · CNF water retention values · CNF aspect ratios

Introduction

The major source of cellulose for nanocellulose production is wood, amongst other sources such as plant biomass, bacteria, algae/macroalgae and tunicates. Wood cellulose is complexed with hemicellulose and lignin, which are embedded within the matrix (Chen 2014). Purity of the cellulose fraction is not necessarily a high priority for industrial use but may become an issue in biomedical applications (Lin and Dufresne 2014; Foster et al. 2018).

For this reason, bacterial nanocellulose (BNC), which is produced de novo from cultures of the bacterium, *Gluconacetobacter xylinus*, is preferred for biomedical applications because of its inherent purity (Lin and Dufresne 2014; Klemm et al. 2018). However, the cost of producing bacterial nanocellulose continues to be a challenge amidst many efforts made in this area, such as the combination of the static and agitated methods of production known as the Horizontal Lift Reactor (HoLiR) (Klemm et al. 2018). A fairly recent review of the problems of the low yield and production cost of BNC revealed the various start-ups, sale and collapse of companies that attempted to commercialise BNC (da Gama and Dourado 2018).

The high cost of energy required in BNC production also applies to cellulose nanofibril (CNF) production from wood and plant biomass. Typical production process of CNF would involve several mechanical shearing pre-treatments (such as pulp refining, milling, beating and dispersing) (Spence et al. 2011), several chemical, biological and swelling pre-treatments (such as 2,2,6,6-Tetramethylpiperidine-1-oxyl (TEMPO)-mediated oxidation (Isogai et al. 2011), carboxymethylation (Wågberg et al. 2008; Im et al. 2018), periodate oxidation (Liimatainen et al. 2012), quaternary ammonium chloride-based modification (Shimizu et al. 2014), enzyme hydrolysis, urea-based microemulsion (Carrillo et al. 2014), ionic liquids (Ninomiya et al. 2018), deep eutectic liquids (Yu et al. 2019) and morpholine swelling (Onyianta et al. 2018)). These pre-treatments are aimed at reducing the effects of intermolecular, intramolecular and hydrophobic forces present in cellulose through changes in surface chemistry of cellulose, partial hydrolysis and swelling. These help to reduce clogging of the fibrillation instrument's interaction chamber. Carrillo et al. (2014) categorically reported that it was not possible to process wood cellulose suspensions that have not undergone any form of pre-treatment.

Even with pre-treatments, homogenisers and high shear processors require the use of a low-solid-content cellulose suspensions (usually between 0.5 and 2 wt. %) during processing. This is to avoid issues related to the pumping of highly viscous suspensions (Spence et al. 2011). In addition, repeated passes through the mechanical fibrillation instrument must be carried out in order to obtain good quality CNF material. Typical examples include 45 passes through a high-pressure homogeniser (also known as

microfluidiser) using unmodified kraft wood cellulose suspension at 0.5 wt. % (Taheri and Samyn 2016) and the successive four-step CNF production from wood cellulose suspension involving a refining step, an enzymatic treatment step, a second refining step, and a high-pressure homogenisation step (Pääkko et al. 2007). The high-pressure homogenisation step was carried out at 2 wt. %, for three passes through the 400 µm and 200 µm interaction chambers and five passes through the 200 µm and 100 µm chambers. Another example is the enzymatic pre-treatment of *Cladophora glomerata* algae followed by 10 or 20 passes with a 200 µm chamber and 10 or 20 additional passes with an 87 µm chamber of a high-pressure processor at 0.2 wt. % (Xiang et al. 2016). These extensive pre-treatments and processing add to the high cost of CNFs and in most cases adversely affect crystallinity and thermal properties (Eyholzer et al. 2010).

Macroalgae such as the cladophorales green algae are known source of cellulose in variable amounts (Mihranyan 2011; Wei et al. 2013; Xiang et al. 2016). The brown seaweed *Saccharina* (*Laminaria*) japonica (Liu et al. 2017; He et al. 2018) has also been recently exploited for cellulose and nanocellulose production. *Laminaria hyperborea* (LH) is a brown seaweed prevalent in the north east Atlantic region (Tyler-Walters 2007) and traditionally used for alginate extraction (Moen et al. 1997). Cellulose accounts for 11% dry matter of *Laminaria hyperborea* (Schiener et al. 2015). This is an untapped source of cellulose which can be harnessed for nanocellulose production for biomedical and other high value applications. Procedures are well established for the extraction of the soluble alginate component from seaweed, leaving behind the insoluble cellulose fraction which is typically regarded as a waste product or low value co-product. Although extraction procedures typically use acid and alkali treatment, as was the case with the material supplied here (Macinnes 2016), these processes are used to extract the alginate and so using the waste cellulose fraction requires no further use of harsh chemicals than those already in place for industrial alginate production. The commercial potential of the cellulose fraction for conversion to high value CNF material has not been realised and is the subject of this study.

Herein, we report the production of cellulose nanofibrils from extracted LH cellulose using high pressure homogenisation. The cellulose supplied required no form of pre-treatment to facilitate fibrillation and only minimal amount of mechanical shearing was needed to produce high quality CNFs, thus providing a zero waste low energy alternative to existing CNFs processes with very high levels of mechanical processing. The surface chemistry of the LH cellulose was studied using Fourier transform infrared spectrophotometry to identify the surface groups and cellulose crystalline polymorph. Variations in the crystallinity indices, viscoelastic properties, water retention values as a function of the number passes through the high-pressure homogeniser were studied. Furthermore, the viscoelastic properties, water retention values and morphological properties of LH cellulose processed at higher solid contents were studied. The aspect ratio and thermal stability of the resulting CNFs were also investigated.

Experimental

Materials

Never dried cellulose from *Laminaria hyperborea* seaweed, 19–20 wt. % solid content was supplied by Marine Biopolymers Ltd (Ayrshire, Scotland). Hydrochloric acid (HCl), sodium chloride (NaCl), and sodium hydroxide (NaOH), were received from Sigma-Aldrich, UK. All chemicals were reagent grade and used without further purification. Ultrapure water (Purelab Option-Q, Class 1 water system, ELGA) was used in all the experiments.

Total acidic group analysis by conductometric titration method

Conductometric titration was used to measure the total acidic group content on the cellulose materials, to determine the extent of residual alginate complexed with the cellulose. While the presence of residual amounts of alginate is unlikely to hinder most CNFs applications, conductometric titration is assessed here as a quality control measure and to determine the extent of washing required to drive the alginate fraction down to a consistent residual level. The as received never dried cellulose was dispersed in 0.5 M NaCl and washed in water to remove any free alginate. Prior to the titration, the LH cellulose was dispersed in

0.1 M HCl for 15 min to protonate any acidic groups. It was then washed thoroughly with water until the conductivity was below 5 µS/cm. 0.2 g of the protonated cellulose was added to 98 ml of water having 2 mL of 0.05 M NaCl. The mixture was stirred and equilibrated for 30 min before being titrated with 0.05 M NaOH. This conductometric titration method was adapted from SCAN-CM 65:02, (2002) test and carried out three times. The average total acidic groups content of the seaweed cellulose was 78 ± 1 µmol/g.

Fourier transform infrared spectrophotometry (FTIR)

Infrared spectra were recorded in transmission mode, in KBr pellets, on a Bruker ALPHA FT-IR spectrophotometer with a resolution of 4 cm^{-1} and an absorbance range of 4000–400 cm^{-1}. The quantity of the sample and KBr in the pellets were 2 mg/200 mg. Five recordings were performed for each sample after successive milling, and the evaluations were further made taking into consideration the average spectrum. Spectral processing was performed using the Grams 9.1 program (Thermo Fisher Scientific).

LH cellulose mechanical processing

Mechanical fibrillation was carried out on LH cellulose material using a PSI-20 high pressure homogenisation (Adaptive Instruments, UK). 1 wt. % aqueous cellulose suspension was passed once through the 200 µm z-shaped interaction chamber and 1–5 times through the 100 µm z-shaped interaction chamber at 170 MPa. This was to study the effect different number of passes on the degree of cellulose fibrillation. Different percentage weights of aqueous cellulose suspensions (0.5, 1, 2 and 3 wt. %) were also given 1 pass through the 200 µm and 100 µm z-shaped interaction chambers at 170 MPa to determine an optimum percentage loading to obtain cellulose nanofibrils.

X-ray diffraction (XRD)

X-ray diffractograms were collected from unprocessed and processed (1–5 passes) samples with Bruker D8 Advance X-ray diffractometer (Germany) using the Cu-Kα radiation (λ 0.1542 nm). A parallel beam with Gobel mirror and a Dynamic Scintillation detector, an accelerating voltage of 40 kV and a current of 30 mA were used within a scanning range of 5°–40° (2θ).

To estimate the degree of crystallinity, the diffractograms were deconvoluted with Voight profile (amorphous background) and mixed Gaussian–Lorenzian profiles (crystalline regions). After deconvolution, the crystalline index can be calculated with the equation proposed by Hermans and Weidinger (1948) and further used by many researchers (Popescu et al. 2007, 2012; Mendoza et al. 2019).

$$Cr.I.\% = \frac{A_{cr}}{A_t} * 100 \quad (1)$$

Here, Cr.I.% is the crystallinity degree, A_{cr} is the sum of signal areas (1−10), (110), (200), (102) and (004), and A_t is the total area under diffractogram.

Linear viscoelastic measurements

Linear viscoelastic measurements were carried on LH cellulose and LHCNFs to determine the effect of increasing number of passes on the storage modulus and the effect of increasing cellulose solid content on the storage modulus of the cellulose nanomaterials. The measurements were carried out using a serrated concentric cylinder geometry, having an inner diameter of 24 mm and outer diameter of 26 mm, attached on AR-G2 rheometer (TA Instruments, USA). The first step of measurement involved a pre-shear regime at a shear rate of 100 s^{-1} for 100 s to clear sample and loading history. The samples were allowed to rest for 10 min through a time sweep at 50 rad s^{-1} and 0.05–0.1% strain. Amplitude sweeps were then carried from 0.01 to 100 Pa at an angular frequency of 50 $rads^{-1}$. The linear viscoelastic region (LVR) for each sample was obtained from the strain versus storage modulus (G')/loss modulus (G'') plots from the amplitude sweeps. Finally, frequency sweeps were carried out at a strain value within the LVR of each sample (0.05–0.1%) from 50 to 0.5 rad s^{-1}. Samples were tested in triplicates and the average data ± standard deviation are reported.

Water retention values

Water retention value (WRV) experiments were carried out on CNF samples with different number of passes and on those processed at different weight

percentages. The method used herein was adapted from Carrillo et al., (2014). The samples were diluted to 0.5 wt. % and subjected to centrifugation at 2300 rpm for 30 min. The supernatant was decanted, and the wet slurries weighed and dried overnight at 105 °C. The dried samples were weighed and WRV were determined using Eq. 2.

$$WRV = \left(\frac{W_{wet} - W_{dry}}{W_{dry}}\right) * 100 \quad (2)$$

Here, W_{wet} and W_{dry} are the weight of the wet slurry and the dried material, respectively. Three replicates were carried out and an average WRV was obtained.

Field emission scanning electron microscopy

Scanning electron micrographs were acquired for LH cellulose and cellulose nanomaterials processed at various solid contents using S4800 FE-SEM, (Hitachi, Japan). Samples were homogenised and diluted to form 0.0001 wt. % solution before being dropped on a freshly cleaved mica disc (muscovite, 9.9 mm diameter and 0.22–0.27 mm thickness, Agar Scientific, UK) that was attached on an FE-SEM aluminium stub. All samples were dried overnight at room temperature. The dried samples were gold coated for 90 s using a sputter coater (EMITECH K550X, Quorumtech, UK) and observed with the FE-SEM at 3 kV acceleration voltage. The widths of fibril were measured using ImageJ software (version 1.47, National Institutes of Health, USA).

Aspect ratio estimation by sedimentation experiments

Sedimentation has been used in many studies to estimate the aspect ratios of CNF materials (Zhang et al. 2012; Varanasi et al. 2013; Im et al. 2018; Onyianta et al. 2018). These studies explain the underlying theories: crowding number (CN) and effective medium theories (EMT), which can be related to the aspect ratio (A) using Eqs. 3 and 4 respectively. The connectivity threshold (Φ_c) in wt. % is determined experimentally by dispersing various wt% of CNF in a medium (usually water or salt solution). Upon sedimentation, the height of the sediment (h_s) and the total height of the dispersion (h_0) are measured. The plot of the initial solid content (wt. %) against the relative sediment height (h_s/h_0) is then fitted with the quadratic equation ($ax^2 + bx$). The linear parameter b, which is equal to the connectivity threshold is converted to weight fraction and subsequently to volume fraction using the density of water (1 g/cm^3) and cellulose (1.5 g/cm^3) (Zhang et al. 2012).

1 wt% LHCNF was initially dispersed in 0.1, 0.5, 1, 1.5, 2 M NaCl solution (at 0.06 w/v%), to examine whether or not the small amount of surface charge on the cellulose surface has any effect on sedimentation. The dispersions were allowed to sediment for 72 h, in a 60 mL glass vial, before capturing photographs from which (h_s) and (h_0) were measured using ImageJ software. Since the lowest relative sediment height was obtained in water, subsequent sedimentations were carried out in water at 0.01 wt. % to 0.1 wt. % for 72 h. Φ_c was then determined as stated above. Sedimentation experiments were carried out in triplicate and the average result ± standard deviation was reported.

$$A = 4.9\Phi_c^{-0.5}(CN) \quad (3)$$

$$A = 2.52\Phi_c^{-0.58}(EMT) \quad (4)$$

Thermogravimetric analysis (TGA)

Thermogravimetric analyses were conducted on LH cellulose and the LHCNF-1P sample to determine their thermal behaviour. TGA was carried out using Mettler Toledo TGA/DSC1 Star System (Mettler Toledo, Switzerland). Approximately 10 mg of each sample was heated from 25 to 600 °C at a constant heating rate of 10 °C/min under a constant nitrogen of 80 mL/min.

Results and discussion

Functional group analysis and cellulose polymorphism analysis by FTIR

The infrared spectrum of the LH cellulose is presented in comparison with the spectrum of the Eucalyptus wood cellulose in Fig. 1a. Both spectra show the typical bands assigned to the functional groups present in cellulose structure, with a large band at 3355 cm^{-1}

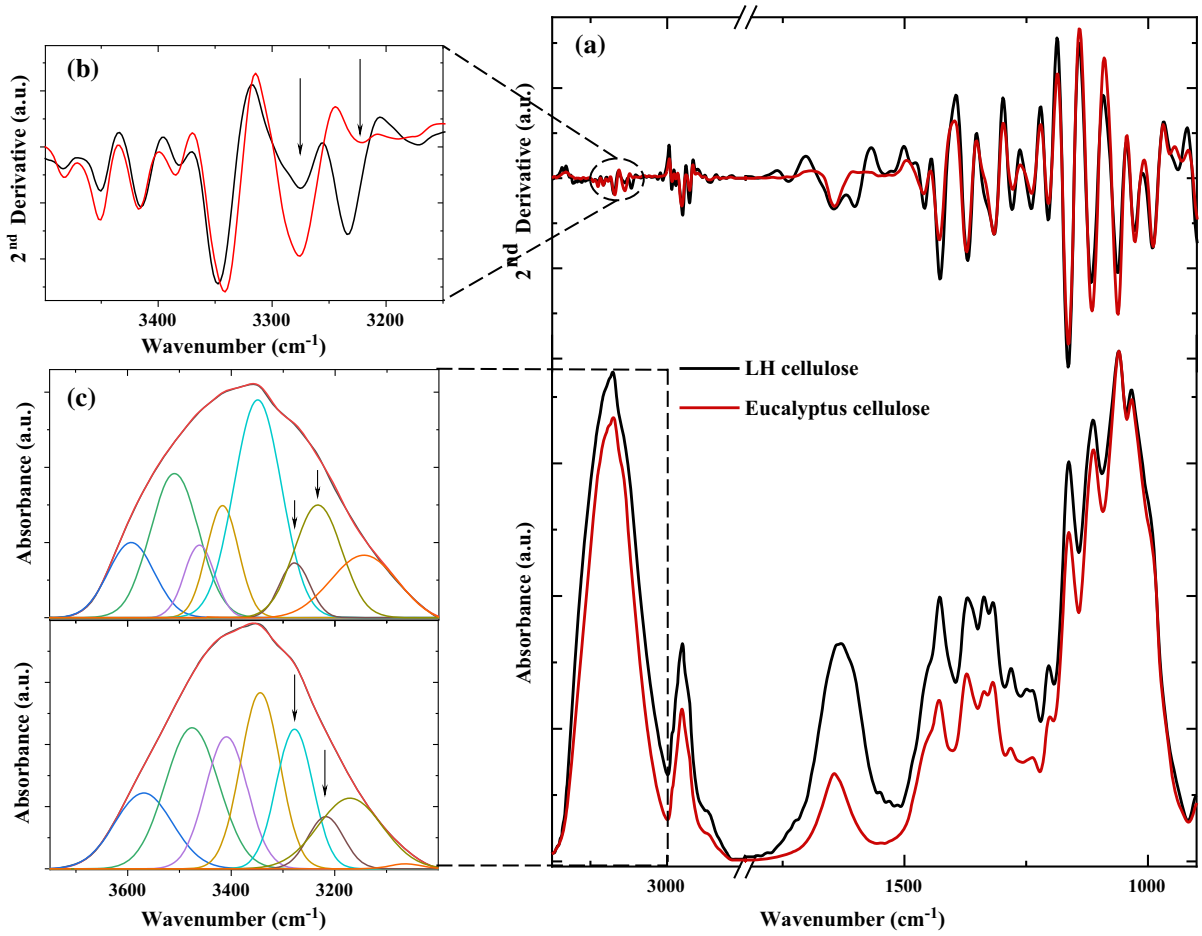

Fig. 1 Infrared spectra and their 2nd derivatives of the LH and Eucalyptus cellulose samples (**a**), zoom of the OH stretching vibration region (**b**) and deconvolution of the OH stretching vibration region (**c**)

which is an envelope of different inter- and intramolecular hydrogen bonds present in cellulose structure, and 2901 cm^{-1} assigned to symmetric and asymmetric stretching vibration of methyl and methylene groups. Details about the exact band position taken from the 2nd derivatives and their assignments are presented in Table 1.

In LH cellulose, the band from 3234 cm^{-1} present higher signal than the band from 3277 cm^{-1}, while in Eucalyptus wood cellulose sample, it is vice versa. In order to identify the ratio between the two cellulose allomorphs, the OH region was deconvoluted (Fig. 1c) and the ratio between the integral area of the two bands was calculated. Therefore, ratio between the cellulose I_β and cellulose I_α for the LH cellulose is about 0.3, while for Eucalyptus cellulose is of about 2.7. In other words, the cellulose I_β/cellulose I_α compositions for LH cellulose is 23%/77%, while for Eucalyptus cellulose is 73%/27%. This result is expected as cellulose from algal sources is known to contain a higher proportion of α cellulose, while cellulose from wood contains a higher proportion of β cellulose (Koyama et al. 1997).

Crystallographic properties of seaweed cellulose and the effect of increase number of mechanical processing on crystallinity index of LHCNF

X-ray diffraction analysis was conducted to evaluate the crystalline structure of the LH samples (Fig. 2). The LH cellulose show a similar X-ray diffractogram pattern identified by Koyama et al. (1997) for the marine red algae *Erythrocladia* (Rhodophyta) I_α rich cellulose and the brown seaweed *Saccharina*

Table 1 Band positions from 2nd derivative spectra and their assignments (Sugiyama et al. 1991; Koyama et al. 1997; Popescu et al. 2007)

Band positions		Band assignments
LH cellulose	Eucalyptus cellulose	
3415	3415	O(2)H···O(6) intramolecular stretching modes
3348	3341	O(3)H···O(5) intramolecular
3276	3276	O(6)H···O(3) intermolecular in cellulose I_β
3233	3221	O(6)H···O(3) intermolecular in cellulose I_α
2969	2966	Asymmetric CH_3 stretching vibration
2942	2943	Asymmetric CH_2 stretching vibration
2899	2903	Symmetric CH_3 stretching vibration
2853	2853	Symmetric CH_2 stretching vibration
1644	1644	Absorbed O–H stretching vibration
1460	1460	C–H deformation vibration
1427	1429	C–H deformation vibration
1371	1373	C–H deformation vibration
1316	1316	C–H stretching vibration
1279	1279	C–O stretching vibration
1240	1239	C–O–C stretching mode of the pyranose ring
1205	1205	C–O–C stretching mode of the pyranose ring
1163	1163	C–O–C stretching vibration in cellulose
1117	1115	Glucose ring stretching vibration
1062	1062	C–O stretching mainly from C(3)–O(3)H
1027	1027	C–O stretching ring
989	989	C–O stretching vibration
938	929	β-Glucosidic linkage between the sugar units

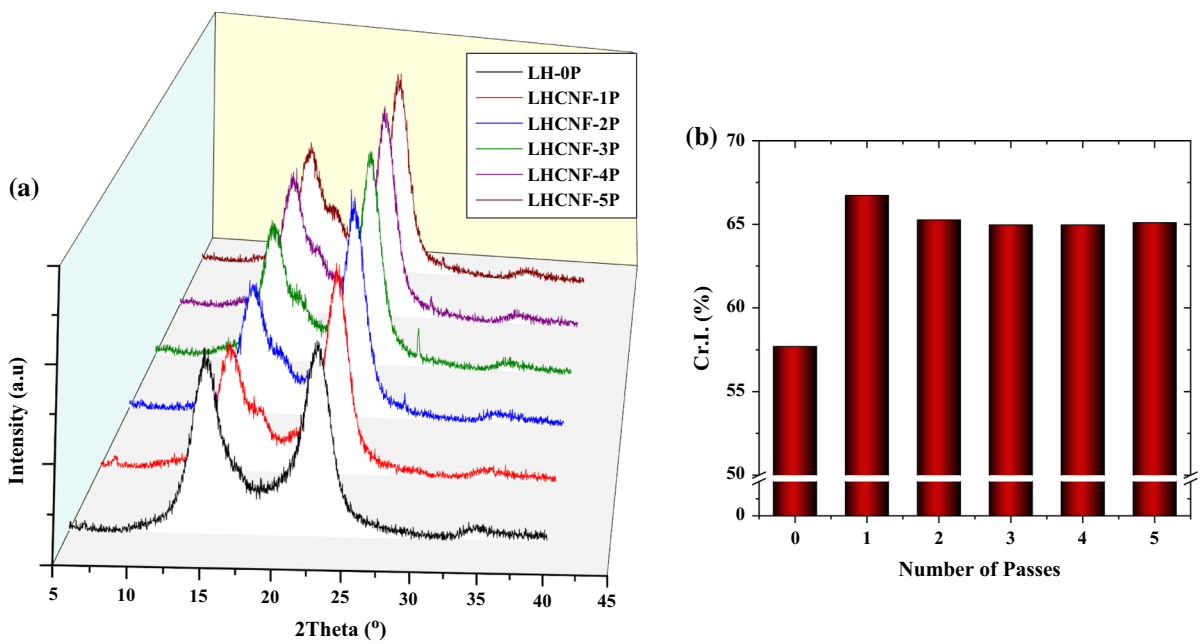

Fig. 2 XRD patterns (**a**) and crystallinity degrees (**b**) of LH cellulose and LHCNFs

(Laminaria) japonica (He et al. 2018), indicating that LH cellulose is rich in I_α allomorph. This observation is in correlation with the one from the FT-IR analysis (see "Functional group analysis and cellulose polymorphism analysis by FTIR" section).

The diffractograms exhibit signals at $2\theta = 14.3°$, 16.5°, 20.3°, 22.7°, and 34.6° corresponding to the (100), (010), (10−2), (110) and (11−4) crystallographic planes, which are in agreement with the characteristic diffraction peaks of cellulose I, albeit I_α allomorph typical of algae (French 2014). The (100) and (010) crystallographic planes are overlapped and the peak from 16.5° (i.e. (010) crystallographic plane) is slightly observable. Further, the peak from 20.6° is merged with the sharp signal from 22.7°.

Figure 2a shows the overlay of the XRD patterns from LHCNF-0P to LHCNF-5P. The number of passes induce a small variation of the intensities of the crystalline signals. Firstly, the peak from 14.3° decreased with increasing number of passes, while the peak from 22.7° is observed to increase when compared with the unprocessed LH cellulose. Subsequent passes (i.e. LHCNF-2P to 5P) resulted in a slight decrease and levelling off in peak intensity. Also, the signal from 16.5° is more visible with increase of the number of passes. This might be due to the breaking up of the structure because of the mechanical processing, decreasing the preferred orientation often manifested by native samples of cellulose I_α. As the number of treatments increased, the relative intensities in the diffraction patterns tended towards the calculated intensities of randomly oriented crystallites of cellulose I_α (French 2014).

The deconvolution of the diffractograms with the Voight profile (amorphous background) and the mixed Gaussian–Lorenzian profiles (crystalline regions) to calculate the crystallinity degrees proved to be a good approach as the reduced Chi squared for all deconvoluted curves was of $\chi^2 \leq 0.1$. The crystallinity degrees are shown in Fig. 2b for LH cellulose and LHCNF-1P to 5P. The crystallinity degree of LH cellulose was 58% and slightly lower than that reported for the brown seaweed *Laminaria japonica* (67%, using the Segal method) (Liu et al. 2017). After the first pass through the mechanical processor however, the Cr.I.% increased to 66.7% from 58%. Similar initial increase in crystallinity degree with increase in number of passes was observed for wood cellulose by Taheri and Samyn (2016). Typically, extended mechanical treatments reduce crystallinity significantly. However, further increases in the number of passes led to an insignificant 2% decrease and levelling off in the Cr.I.% values. The initial increase in crystallinity after a single pass and maintenance of crystallinity thereafter may be a feature of high shear homogenisation by delaminating and separating the cellulose fibres, opening them up to more effective crystallinity analysis. Thus, the pulverisation effects of grinding, ball milling or other mechanical processes which reduce crystallinity are not present.

Linear viscoelastic properties and water retention values of LHCNF

The degree of mechanical processing of cellulose fibres is known to affect the linear viscoelastic properties and shear viscosity properties of the resulting nanofibres (Nechyporchuk et al. 2016). In this study the effects of the number of passes on the linear viscoelastic properties were studied using amplitude sweeps and frequency sweeps measurements. For these tests, amplitude sweeps were carried out to identify the strain value, within the linear viscoelastic region that is needed for the frequency sweep tests. The results from the frequency sweep experiments are summarised in Fig. 3 for the LH cellulose and for LHCNF-1P to 5P samples.

For all the samples tested, the storage moduli were greater than the loss moduli, even for unprocessed cellulose sample. In addition, all samples showed a storage modulus which is relatively independent of angular frequency. These are indications of the elastic nature of the LHCNF materials. It should be noted that the rheological measurement of unprocessed cellulose suspensions from wood and plant sources are often impossible due to the prevalent rapid sedimentation of the fibres in aqueous suspension. However, the LH cellulose fibres are highly swelling in water and can maintain a stable suspension at 1 wt. %.

A single pass of the cellulose fibres through the high-pressure homogeniser led to an 8-fold increase in storage modulus. Further passes (up to 5 passes) did not lead to significant increase in storage modulus that would justify the additional energy consumption. It is worth noting that the storage modulus of 1 pass CNF from the seaweed cellulose is up to 50% greater than the storage modulus of CNF from wood pulp that has undergone aqueous morpholine pre-treatment and 5

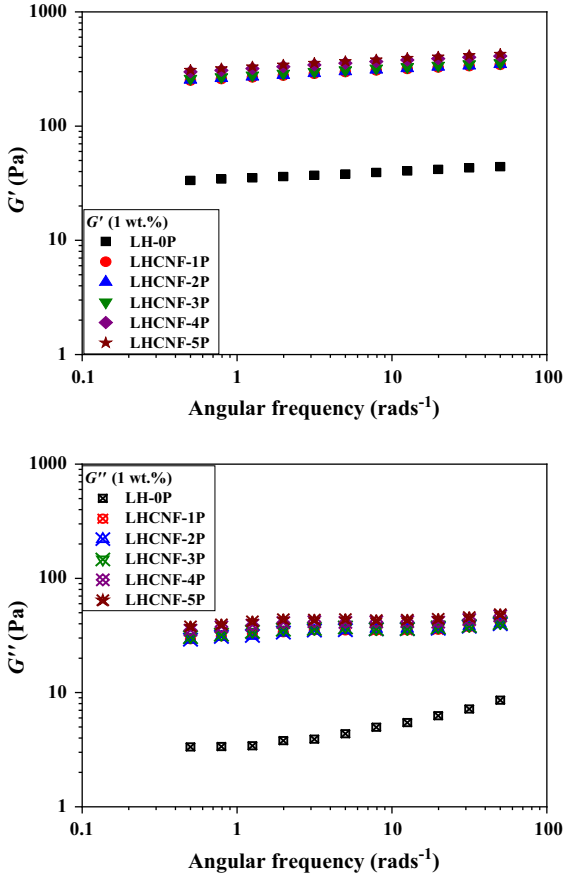

Fig. 3 Frequency sweeps of LH cellulose and 1 to 5-pass LHCNF samples showing the effect of increasing degree of mechanical fibrillation on G' and G''

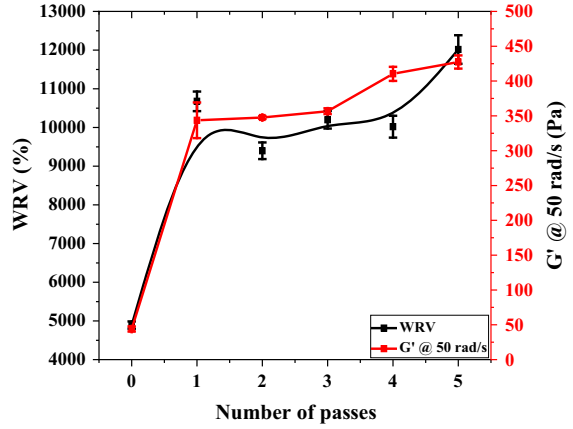

Fig. 4 Effects of increased number of passes on water retention values and storage modulus

passes through the high pressure homogeniser (Onyianta et al. 2018).

The increase in fibrillation of cellulose is expected to transform tightly matted cellulose fibres to a loose, yet interconnected network of fibrils, capable of retaining more water than the cellulose fibres. Water retention tests were used to investigate the impact of increased number of passes on the degree of fibrillation on the water retention capability. The water retention values are shown in Fig. 4, where they are overlaid with the storage modulus of each sample at 50 rad s^{-1}.

The trend observed with storage modulus when increasing the number of passes was also seen with the water retention values. The water retention value of the cellulose nanofibrils after a single pass was doubled in comparison to the unprocessed cellulose fibres. The water retention values of 2-pass to 4-pass samples remained broadly similar, while a slight increase in water retention (12%) was observed for the 5-pass sample. Again, this increase was not considered to be commensurate with the energy required for the 5-pass sample.

Subsequently, LH cellulose fibres were given a single pass through the high-pressure homogeniser at different cellulose solid contents in weight percentages. Processing of cellulose at a higher solid content is desired, especially in large scale production, because it can cut down processing time and energy cost. Therefore, the effects of increase in cellulose processing solid content on the rheological properties, water retention values and morphological properties were studied.

The effects of various cellulose processing solid contents on the viscoelastic properties of the nanomaterials were studied from rheograms obtained from frequency sweep measurements, shown in Fig. 5. The storage moduli of the samples processed at different cellulose solid contents are also higher than the loss moduli and independent of the angular frequency. There was a continuous and rapid increase in storage modulus (clearly illustrated in Fig. 6) with increase in cellulose content. This is expected as the presence of greater amount of fibrils would result in high interconnection of these fibrils (Nechyporchuk et al. 2014).

The effect of the cellulose processing loading on water retention values of the LHCNF is also shown in Fig. 6. WRV is expected to reveal whether high solid content processing of cellulose affected the water retention capability of the CNF, which can then be

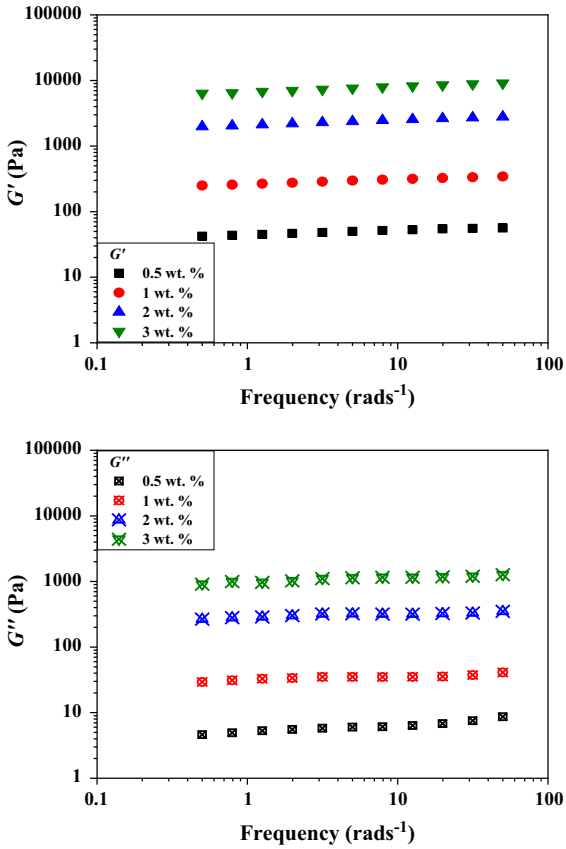

Fig. 5 Frequency sweeps of LHCNF samples processed at different cellulose weight loadings

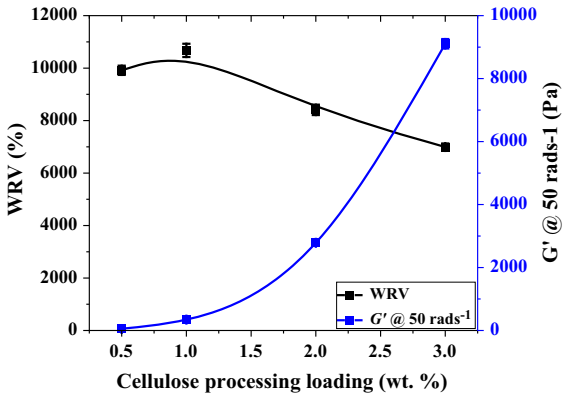

Fig. 6 Changes in the storage moduli and WRV of LHCNF with increasing cellulose processing solid content

translated to the degree of fibrillation of the cellulose materials. Based on the data from the WRV, there is a clear picture that the best results are obtained by processing at lower solid contents. As the cellulose solid content increases, the level of fibrillation become hindered because of the increase in storage modulus. It is unlikely that the fibres would have the same amount of interaction in the chambers during high shear processing, hence, possibly giving a higher portion of cellulose microfibrils.

Morphological analysis of LH cellulose nanofibrils

The morphology of the LHCNFs were examined from FE-SEM images, from which the widths of the fibrils were also measured. The morphology of the LH cellulose at 5 k and 25 k magnifications are shown in Fig. 7a, b respectively. The magnified image of LH cellulose shows highly matted and interconnected fibres having void spaces. This morphology could explain the highly moisture absorbing nature and the ability of LH cellulose to maintain stable suspension after a mild mechanical shearing with Ultraturrax rotor–stator disperser.

The effect of the single pass through the 200 µm and 100 µm interaction chambers on the morphology of the resulting LHCNF-1P is stark as can be seen in Fig. 7c (25 k magnification) and Fig. 7d (45 k magnification). The morphology of the single pass sample at 1 wt. % is that of individualised yet interconnected fibrils spanning across the field of view of the image. Higher magnification images (45 k) show comparable morphologies across all samples processed at different cellulose solid contents (Fig. 7d, f, h). However, the low magnification images (25 k) of the 2 wt. % and 3 wt. % samples (Fig. 7e, g) show the presence of larger fibrils, which explains the reduced water retention values for these samples. The properties of the samples processed at high solid contents are still regarded to be of good quality if one should consider that these samples did not undergo any form of mechanical, biological or chemical pre-treatments as would be required from other sources of cellulose for CNF production.

The average fibril width of LHCNF-1P as measured from FE-SEM images is 19 ± 5 nm, having a minimum width of 7 nm and a maximum width of 63 nm. The length of the fibrils could not be measured because of the inherent long fibrillar nature of the LHCNF samples even at lower solid content at which the samples were prepared for FE-SEM analysis. Therefore, the aspect ratio of the LHCNF were estimated using the sedimentation method and presented in

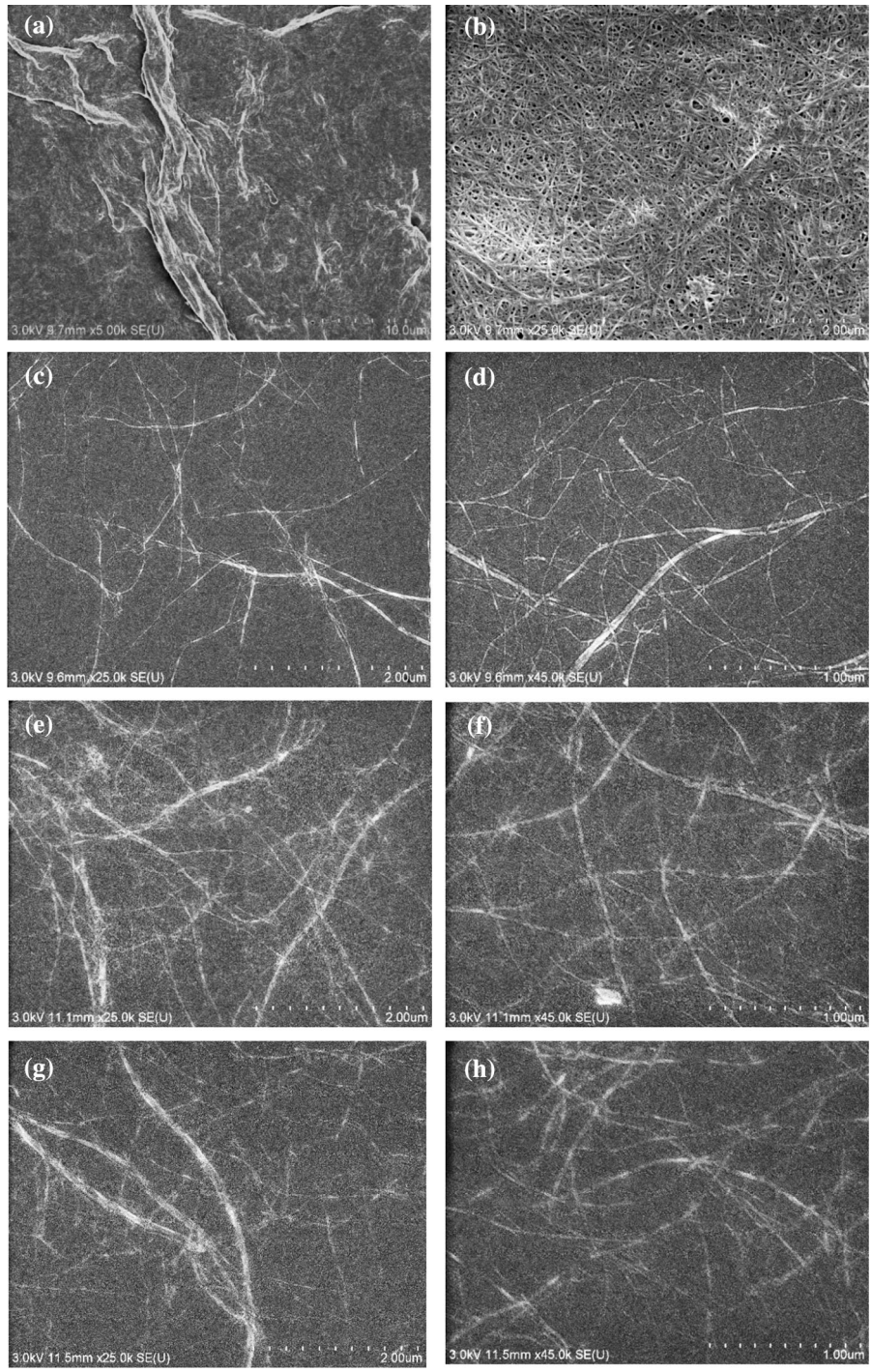

Fig. 7 FE-SEM images of LH cellulose at 5 k (**a**) and 25 k (**b**) magnifications and LHCNF-1P 1 wt. % [25 k (**c**) and 45 k (**d**)], 2 wt. % [25 k (**e**) and 45 k (**f**)] and 3 wt. % [25 k (**g**) and 45 k (**h**)]

"Aspect ratio estimation of LH cellulose nanofibrils using sedimentation approach" section.

Aspect ratio estimation of LH cellulose nanofibrils using sedimentation approach

The plot of relative sediment height versus CNF solid content is shown in Fig. 8 with a photographic insert

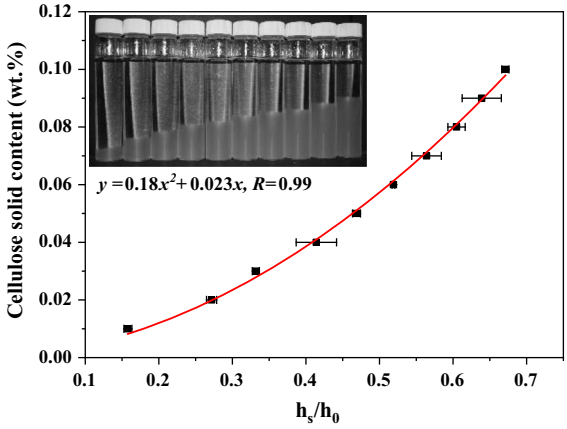

Fig. 8 Quadratic fit of relative sediment height against initial CNF solid content and representative photographic insert of sedimentation vials

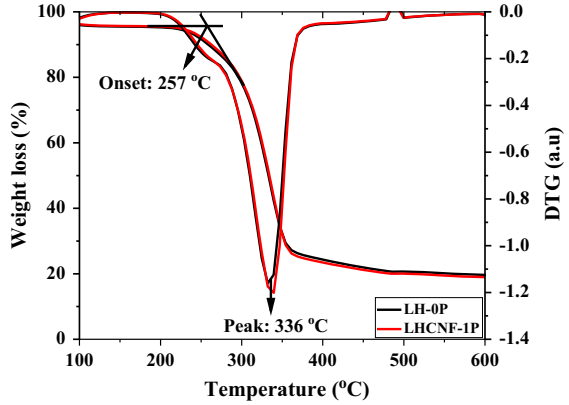

Fig. 9 TGA and DTG thermograms of LH cellulose and LHCNF-1P showing the onset and peak degradation temperatures

of the sedimentation vials. Upon fitting the plot with a nonlinear quadratic fit, the linear component of the fit is equivalent to the connectivity threshold. The CN and EMT aspect ratios as calculated using Eqs. 3 and 4 are 394 ± 10 and 408 ± 10 respectively. The CN aspect ratio of LHCNF is more than twice the values reported for unmodified wood cellulose CNFs (125–161) (Varanasi et al. 2013; Onyianta et al. 2018). The long fibrillar nature of LHCNF is evident from the SEM images shown in Fig. 7. This property could be an inherent property or as a result of the mild mechanical processing condition. The high aspect ratio LHCNF alongside the identified high storage modulus indicate that it would be a good structuring material in composite formulations.

Thermogravimetric properties of LH cellulose and LHCNF

Thermogravimetric analysis provides an insight on the behaviour of a polymer material at elevated temperature. The thermal properties of the LH cellulose (LH-0P) and LHCNF-1P were studied. The thermogravimetric curves and derivative thermogravimetric (DTG) curves of these samples are shown in Fig. 9.

The onset degradation temperature and the peak degradation temperature of the LH cellulose before and after a single pass through the mechanical instrument remained the same at 257 °C and 336 °C respectively. Less intensive mechanical shearing does not significantly impose a detrimental effect on the thermal stability of cellulose compared to chemical treatments as shown by Eyholzer et al. (2010) and Onyianta et al. (2018). Therefore, there was no difference in the thermal properties of LH cellulose and LHCNF-1P. Sun et al. (2020) showed that increase in the number of passes of water hyacinth cellulose nanofibrils does not have any impact on the thermal stability of the CNF. This behaviour is also anticipated for LHCNF-2P to 5P. The onset and peak degradation temperature values reported herein are typical of unmodified cellulose fibres/fibrils (Jonoobi et al. 2015), indicating their suitability as reinforcements in bioplastics like polylactic acid (PLA), which melt between 150 and 200 °C (Signori et al. 2009).

Conclusions

Cellulose nanofibrils from *Laminaria hyperborea* cellulose extract have been extensively characterised for surface properties, crystallinity indices, viscoelastic properties, water retention values, morphological properties, aspect ratios and thermal stability. The inherent porous morphology of LH cellulose results in a material with a high-water absorption, leading to ease of fibrillation without the need for any form of pre-treatment. Only a single pass through the 200 µm and 100 µm interaction chambers of the high-pressure homogeniser was required to produce CNF materials with good crystallinity degree, high storage moduli, high water retention values, good morphological properties, high aspect ratio and good thermal

properties. These good qualities were also identified for CNFs processed at higher cellulose loading, which would result to an overall reduction in the cost of LHCNF production. The low energy requirements and zero waste aspects of this process provide an attractive proposition for commercialising CNF from seaweed as a direct replacement in wood and bacterial nanocellulose applications. This process creates CNF which is unmodified and so may be more useful for hydrophobic applications than with wood derived material which has undergone chemical pre-treatments. The inherent porous nature of the LH cellulose which makes it easy to process at low energy demands similarly lends itself well to modification of the CNF surface. Surface modification would help to effect efficient re-suspension from dried material and to increase the range of high value applications.

Laminaria hyperborea is a wild seaweed and is not currently cultivated. As a result, there is a maximum sustainable yield. In terms of current alginate production, estimated to be in the region of 30,000 tonnes per year, the yield of cellulose available for conversion to CNF is likely to be in the region of 5000 to 8000 tonnes per year. Brown seaweed cultivation is however an active area of research and our technology may be applicable to other wild brown seaweeds such as Sargassum, which is available in much larger quantities and is widely regarded as an invasive species.

Acknowledgments The authors would like to thank Zero Waste Scotland and the School of Engineering and Built Environment, Edinburgh Napier University for funding this research and Marine Biopolymers Ltd for providing the extracted cellulose material.

References

Carrillo CA, Laine J, Rojas OJ (2014) Microemulsion systems for fiber deconstruction into cellulose nanofibrils. ACS Appl Mater Interfaces 6:22622–22627. https://doi.org/10.1021/am5067332

Chen H (2014) Biotechnology of lignocellulose: Theory and practice. Springer, Berlin

da Gama FMP, Dourado F (2018) Bacterial nano cellulose: what future? BioImpacts 8:1–3. https://doi.org/10.15171/bi.2018.01

Eyholzer C, Bordeanu N, Lopez-Suevos F et al (2010) Preparation and characterization of water-redispersible nanofibrillated cellulose in powder form. Cellulose 17:19–30. https://doi.org/10.1007/s10570-009-9372-3

Foster EJ, Moon RJ, Agarwal UP et al (2018) Current characterization methods for cellulose nanomaterials. Chem Soc Rev 47:2609–2679. https://doi.org/10.1039/c6cs00895j

French AD (2014) Idealized powder diffraction patterns for cellulose polymorphs. Cellulose 21:885–896. https://doi.org/10.1007/s10570-013-0030-4

He Q, Wang Q, Zhou H et al (2018) Highly crystalline cellulose from brown seaweed Saccharina japonica: isolation, characterization and microcrystallization. Cellulose 25:5523–5533. https://doi.org/10.1007/s10570-018-1966-1

Hermans PH, Weidinger A (1948) Quantitative X-ray investigations on the crystallinity of cellulose fibers. A background analysis. J Appl Phys 19:491–506. https://doi.org/10.1063/1.1698162

Im W, Lee S, Rajabi Abhari A et al (2018) Optimization of carboxymethylation reaction as a pretreatment for production of cellulose nanofibrils. Cellulose 25:1–11. https://doi.org/10.1007/s10570-018-1853-9

Isogai A, Saito T, Fukuzumi H (2011) TEMPO-oxidized cellulose nanofibers. Nanoscale 3:71–85. https://doi.org/10.1039/C0NR00583E

Jonoobi M, Oladi R, Davoudpour Y et al (2015) Different preparation methods and properties of nanostructured cellulose from various natural resources and residues: a review. Cellulose 22:935–969. https://doi.org/10.1007/s10570-015-0551-0

Klemm D, Cranston ED, Fischer D et al (2018) Nanocellulose as a natural source for groundbreaking applications in materials science: today's state. Mater Today 21:720–748. https://doi.org/10.1016/j.mattod.2018.02.001

Koyama M, Sugiyama J, Itoh T (1997) Systematic survey on crystalline features of algal celluloses. Cellulose 4:147–160. https://doi.org/10.1023/A:1018427604670

Liimatainen H, Visanko M, Sirviö JA et al (2012) Enhancement of the nanofibrillation of wood cellulose through sequential periodate-chlorite oxidation. Biomacromol 13:1592–1597. https://doi.org/10.1021/bm300319m

Lin N, Dufresne A (2014) Nanocellulose in biomedicine: Current status and future prospect. Eur Polym J 59:302–325. https://doi.org/10.1016/j.eurpolymj.2014.07.025

Liu Z, Li X, Xie W, Deng H (2017) Extraction, isolation and characterization of nanocrystalline cellulose from industrial kelp (*Laminaria japonica*) waste. Carbohydr Polym

173:353–359. https://doi.org/10.1016/j.carbpol.2017.05.079
Macinnes D (2016) Method of processing seaweed and related products. European Patent Office EP3068804A1, pp 1–57
Mendoza DJ, Browne C, Raghuwanshi VS et al (2019) One-shot TEMPO-periodate oxidation of native cellulose. Carbohydr Polym 226:115292. https://doi.org/10.1016/j.carbpol.2019.115292
Mihranyan A (2011) Cellulose from cladophorales green algae: from environmental problem to high-tech composite materials. J Appl Polym Sci 119:2449–2460. https://doi.org/10.1002/app.32959
Moen E, Larsen B, Østgaard K (1997) Aerobic microbial degradation of alginate in *Laminaria hyperborea* stipes containing different levels of polyphenols. J Appl Phycol 9:45–54. https://doi.org/10.1023/A:1007956230761
Nechyporchuk O, Belgacem MN, Pignon F (2014) Rheological properties of micro-/nanofibrillated cellulose suspensions: wall-slip and shear banding phenomena. Carbohydr Polym 112:432–439. https://doi.org/10.1016/j.carbpol.2014.05.092
Nechyporchuk O, Belgacem MN, Pignon F (2016) Current progress in rheology of cellulose nanofibril suspensions. Biomacromol 17:2311–2320. https://doi.org/10.1021/acs.biomac.6b00668
Ninomiya K, Abe M, Tsukegi T et al (2018) Lignocellulose nanofibers prepared by ionic liquid pretreatment and subsequent mechanical nanofibrillation of bagasse powder: application to esterified bagasse/polypropylene composites. Carbohydr Polym 182:8–14. https://doi.org/10.1016/j.carbpol.2017.11.003
Onyianta AJ, Dorris M, Williams RL (2018) Aqueous morpholine pre-treatment in cellulose nanofibril (CNF) production: comparison with carboxymethylation and TEMPO oxidisation pre-treatment methods. Cellulose 25:1047–1064. https://doi.org/10.1007/s10570-017-1631-0
Pääkko M, Ankerfors M, Kosonen H et al (2007) Enzymatic hydrolysis combined with mechanical shearing and high-pressure homogenization for nanoscale cellulose fibrils and strong gels. Biomacromol 8:1934–1941. https://doi.org/10.1021/bm061215p
Popescu CM, Popescu MC, Singurel G et al (2007) Spectral characterization of eucalyptus wood. Appl Spectrosc 61:1168–1177. https://doi.org/10.1366/000370207782597076
Popescu CM, Larsson PT, Olaru N, Vasile C (2012) Spectroscopic study of acetylated kraft pulp fibers. Carbohydr Polym 88:530–536. https://doi.org/10.1016/j.carbpol.2011.12.046
SCAN-CM 65:02 (2002) Total acidic group content. In: Scandinavian Pulp, Paper, and Board Testing committee. http://www.kemesta.fi/document.php/1/102/cm_65-02.pdf/cf67249080953749768b08f7e2eb88af. Accessed 1 Mar 2019
Schiener P, Black KD, Stanley MS, Green DH (2015) The seasonal variation in the chemical composition of the kelp species *Laminaria digitata*, *Laminaria hyperborea*, *Saccharina latissima* and *Alaria esculenta*. J Appl Phycol 27:363–373. https://doi.org/10.1007/s10811-014-0327-1
Shimizu M, Saito T, Fukuzumi H, Isogai A (2014) Hydrophobic, ductile, and transparent nanocellulose films with quaternary alkylammonium carboxylates on nanofibril surfaces. Biomacromol 15:4320–4325. https://doi.org/10.1021/bm501329v
Signori F, Coltelli M-B, Bronco S (2009) Thermal degradation of poly(lactic acid) (PLA) and poly(butylene adipate-co-terephthalate) (PBAT) and their blends upon melt processing. Polym Degrad Stab 94:74–82. https://doi.org/10.1016/J.POLYMDEGRADSTAB.2008.10.004
Spence KL, Venditti RA, Rojas OJ et al (2011) A comparative study of energy consumption and physical properties of microfibrillated cellulose produced by different processing methods. Cellulose 18:1097–1111. https://doi.org/10.1007/s10570-011-9533-z
Sugiyama J, Persson J, Chanzy H (1991) Combined infrared and electron diffraction study of the polymorphism of native celluloses. Macromolecules 24:2461–2466. https://doi.org/10.1021/ma00009a050
Sun D, Onyianta AJ, O'Rourke D et al (2020) A process for deriving high quality cellulose nanofibrils from water hyacinth invasive species. Cellulose 27:3727–3740
Taheri H, Samyn P (2016) Effect of homogenization (microfluidization) process parameters in mechanical production of micro- and nanofibrillated cellulose on its rheological and morphological properties. Cellulose 23:1221–1238. https://doi.org/10.1007/s10570-016-0866-5
Tyler-Walters H (2007) Tangle or cuvie (*Laminaria hyperborea*). In: Marine life information network biology and sensitivity key information review
Varanasi S, He R, Batchelor W (2013) Estimation of cellulose nanofibre aspect ratio from measurements of fibre suspension gel point. Cellulose 20:1885–1896. https://doi.org/10.1007/s10570-013-9972-9
Wågberg L, Decher G, Norgren M et al (2008) The build-up of polyelectrolyte multilayers of microfibrillated cellulose and cationic polyelectrolytes. Langmuir 24:784–795. https://doi.org/10.1021/la702481v
Wei N, Quarterman J, Jin Y-S (2013) Marine macroalgae: an untapped resource for producing fuels and chemicals. Trends Biotechnol 31:70–77. https://doi.org/10.1016/J.TIBTECH.2012.10.009
Xiang Z, Gao W, Chen L et al (2016) A comparison of cellulose nanofibrils produced from *Cladophora glomerata* algae and bleached eucalyptus pulp. Cellulose 23:493–503. https://doi.org/10.1007/s10570-015-0840-7
Yu W, Wang C, Yi Y et al (2019) Choline chloride-based deep eutectic solvent systems as a pretreatment for nanofibrillation of ramie fibers. Cellulose 26:3069–3082. https://doi.org/10.1007/s10570-019-02290-7
Zhang L, Batchelor W, Varanasi S et al (2012) Effect of cellulose nanofiber dimensions on sheet forming through filtration. Cellulose 19:561–574. https://doi.org/10.1007/s10570-011-9641-9